

Transient temperature induced plasmonic crystalMarat Spector and Stanislav Derevyanko^{✉*}*School of Electrical and Computer Engineering, Ben Gurion University of the Negev, Beer Sheva 84105, Israel*

(Received 27 May 2020; revised 7 September 2020; accepted 28 October 2020; published 12 November 2020)

We suggest an easily configurable dynamical method of creating a periodic quasi-2D plasmonic lattice in a metal film by temperature induced variation of the dielectric permittivity. The temperature variations in turn are controlled by two pairs of perpendicular pump beams irradiating the metal surface. By varying the incident angles of the beams one can control the effective spatial periods of the lattice while the erasure time is given by the pulse duration ranging from pico- to nanoseconds. We show that the modulation effect is most prominent in the imaginary part of the metal dielectric function and thus the obtained plasmonic crystal is fully dissipative. We also demonstrate that such crystal displays reduced absorption at the Brillouin zone boundary and calculate the transmission as a function of the transient contrast of the lattice.

DOI: [10.1103/PhysRevB.102.174308](https://doi.org/10.1103/PhysRevB.102.174308)**I. INTRODUCTION**

Photonic crystals have opened new possibilities in the optics of nanosurfaces finding multiple application in light harvesting, manipulation, and material coating [1]. On the other hand they have their counterparts in 2D surface plasmonic crystals (SPC) for surface plasmon polaritons (SPPs) [2,3], a propagating surface electromagnetic waves on a metal-dielectric interface. A common definition of SPC is a periodically structured metal surface with the lattice period on the order of SPP wavelength [3–5]. Periodically corrugated surface of metal-dielectric interface [3,4,6,7] opens band gaps in SPP dispersion law [5,8]. By controlling the periodicity of the lattice the dispersion of SPP modes can be freely designed while different SPP modes can be effectively coupled and/or excited. It is also possible to consider quasi-one-dimensional modulation of the metal surface resulting in SPP Bragg grating [9]. Most of the structures considered in SPC literature are characterized by the following properties: (i) the periodic modulation is performed on the real part of the dielectric function (permittivity) and (ii) the resulting corrugated structures are *permanent* and cannot be reconfigured.

On the other hand there exists a vast area of applications related to matter manipulations by ultrafast laser pulses ranging from ablation to spectroscopy [10–13]. The high intensity pulse interacts with the charge carriers inside the medium (both metallic and dielectric) which leads to a variety of secondary effects related to energy dissipation and diffusion [14] and material processing through laser-induced damage [15]. Different structures can be inscribed in dielectric materials both periodic and nonperiodic [16–19]. The main difference between metal and dielectric media in this respect is the abundance of free carriers residing within the crystal lattice of metal that can be excited by the laser-induced heat source [14,20–22] thus providing the mechanism of modula-

tion of the dielectric function and the response of metal to the probe electromagnetic field [23]. Because of the diffusive temperature relaxation of both the electron and lattice subsystems the resulting structures have a *transient* nature. The particular interest is presented by transient periodic structures or transient Bragg gratings [24–27]. Such structures have potential applications as ultrafast switching components [28,29] with the potential to reach subpicosecond response times.

In our work we show that by using two pairs of crossed beams illuminating the surface of a metal film one can create a transverse transient spatially-periodic structure with controllable periods of the lattice limited by the wavelengths of the inscribing pump beams. The depth of this lattice in metal is shown to be much larger than the penetration depth of an SPP in resonance with the period of the lattice which makes the induced plasmonic crystal quasi-2D. We also show that in the NIR the temperature dependence of the standard Drude model makes the induced transient SPC purely dissipative as the temperature induced modulation affects mostly the imaginary part of the permittivity. In such purely dissipative periodic structures the Bragg resonances at the boundary of the Brillouin zone lead not to the band-gap opening but to the narrow transparency spectral window where the transmittance is higher due to the resonant modulation of the dielectric losses. Such enhanced transmission has been observed, e.g., in acoustics [30] and here we predict it as a transient effect in the temperature-induced dissipative lattice. These structures can therefore be used as effective gating mechanism for SPPs acting as probe waves at the Bragg resonance.

The paper is structured as follows. In Sec. II, we study the properties of the induced temperature modulation by the two pairs of incident beams using a standard two-temperature model. In Sec. III we build a linear theory for the induced temperature changes of the electron and lattice subsystems assuming that these changes are small. Section IV presents the results of full numerical simulations of the two-temperature model in both the 3D and 2D case. In Sec. V, we translate these changes into the variation of the imaginary part of the

*stasd@bgu.ac.il

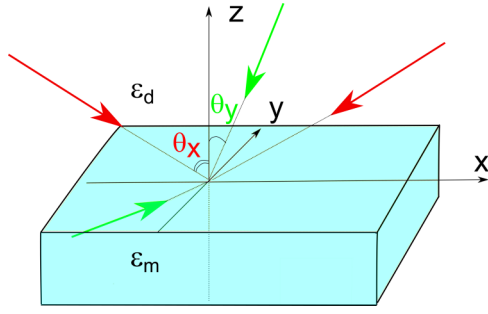


FIG. 1. Geometry of four-beam irradiation of the surface.

dielectric function within the framework of a standard Drude model and study the transparency properties of the resulting structures at the Bragg resonance. The findings are summarized in the Discussion.

II. TEMPERATURE-INDUCED TRANSIENT LATTICE

In order to create a 2D transient lattice we propose irradiating a metal film interface by two pairs of orthogonal pump beams impinging with incident angles θ_x and θ_y —see Fig. 1. For simplicity, we assume both beams to have transverse electric (TE) polarization and assuming symmetric irradiation in each plane the slowly varying envelope of the electric field at the interface can be presented as

$$\begin{aligned} \vec{E}_p(x, y, z = 0, t) &= (A \cos(k \sin \theta_y y + \phi_y) g_1(t), \\ &B \cos(k \sin \theta_x x + \phi_x) g_2(t), 0), \end{aligned} \quad (1)$$

where $g_1(t)$ and $g_2(t)$ are the temporal shapes of the two beams, $\phi_{x,y}$ are the corresponding phase shifts in each polarization, A and B are the amplitudes of the two beams, and $k = 2\pi/\lambda$ is the incident wave number. The pump beams are incident from a dielectric material $\epsilon_d > 0$ occupying the $z > 0$ half-space and the metal dielectric function is complex $\epsilon_m = \epsilon'_m + i\epsilon''_m$ occupying the lower half-space $z < 0$. In what follows we shall assume identical time-synchronised Gaussian pulses so that $g_1(t) = g_2(t) = g(t) = \exp(-t^2/2\tau_p^2)$ although various time-delayed schemes are also possible. Time synchronization can be organized, e.g., by using a beam splitter and equal optical lengths in both arms of the resulting interferometer.

We assume that the film is thick enough to neglect the effects of the substrate and the thickness is much larger than the skin-depth $l \sim 20$ nm in noble metals in NIR. Our results therefore apply equally to the bulk geometry.

Since propagation in metal ($z < 0$) is lossy the incident pump field causes energy dissipation with the rate proportional to the imaginary part of the dielectric permittivity [31]:

$$\begin{aligned} p_{abs}(x, y, z, t) &= \epsilon_0 \epsilon''_m \omega (1 - R) |\vec{E}_p(x, y, t)|^2 / 2 \\ &= p_0 \left(\alpha \cos^2 \left[\pi \frac{x}{\Lambda_x} + \phi_x \right] \right. \\ &\quad \left. + \beta \cos^2 \left[\pi \frac{y}{\Lambda_y} + \phi_y \right] \right) e^{2z/l} g^2(t) \end{aligned} \quad (2)$$

where R is the reflectivity. The reflectivity of noble metals in the NIR region considered here is quite high so that

the amount of power entering a metal film thicker than the skin depth is quite small. However the existing antireflective coating technologies allow one to reduce this reflectivity significantly [32].

The effective lattice periods are given by $\Lambda_{x,y} = \lambda / (2 \sin \theta_{x,y})$ and the power split ratios are $\alpha = |B|^2 / (|A|^2 + |B|^2)$, $\beta = |A|^2 / (|A|^2 + |B|^2)$. The electromagnetic field dissipation then acts as a source for ultrafast heat diffusion in both electronic and lattice subsystems in the film. To model these effects we adopt here the two temperature model (TTM) [14]:

$$\begin{aligned} C_e(T_e) \frac{\partial T_e}{\partial t} &= \nabla \cdot [K_e(T_e, T_l) \nabla T_e] - G(T_e - T_l) + p_{abs}, \\ C_l \frac{\partial T_l}{\partial t} &= \nabla \cdot [K_l(T_l) \nabla T_l] + G(T_e - T_l). \end{aligned} \quad (3)$$

Here, $C_{e,l}$ and $K_{e,l}$ are the heat capacities and thermal conductivities of the electrons and the lattice and G is the electron-phonon coupling factor related to the rate of energy exchange between the electrons and the lattice [33]. The thermal conductivities of the electron and lattice subsystem are given as [34]

$$K_e = \frac{C_e v_F^2}{3\gamma} \quad (4a)$$

$$K_l = \frac{C_l c_s^2}{3\gamma_{e-ph}}, \quad (4b)$$

where v_F represents the Fermi velocity, c_s is the speed of sound, and γ and γ_{e-ph} are temperature-dependent scattering rates defined below in Eq. (14). Note that in general one has $K_l \ll K_e$.

The model (3) adds only the lattice temperature diffusion terms to the original local theory of Ref. [14]. Over the years many enhanced and generalized versions of the TTM have emerged [13,15,27,35]. Most modification relates to the non-local connection between the dissipated energy density p_{abs} in (2) and the source term in (3). For example in Ref. [27] the dissipated electromagnetic energy served not as a direct source in the TTM but was driving the nonthermal (NT) electronic energy for which a purely phenomenological diffusion terms were introduced. It was the latter nonthermal energy that was used as a source driving both temperatures. Here however we prefer to follow a traditional and more established model. In the following section we shall provide an analytical treatment of the TTM when the incident pulses intensity is small so that the induced temperature changes can be found perturbatively.

III. LINEAR THEORY

The system (3) is nonlinear and is generally solved numerically. In order to get some insight of the typical scales and effects an analytical solution can be sought using a perturbation theory. We shall assume that initially both film and the dielectric substrate are at the same equilibrium temperature T^{eq} and the deviation of both subsystems from thermal equilibrium resulting from the irradiation is small. Then we can

TABLE I. Parameters used in the solution of the original (3) and linearized (7) *TTM*.

Parameter	Value	Units	Reference
C_e^{eq}	2.1×10^4	$\text{Jm}^{-3} \text{K}^{-1}$	[34]
C_l	2.5×10^6	$\text{Jm}^{-3} \text{K}^{-1}$	[34]
G	2.5×10^{16}	$\text{Jm}^{-3} \text{K}^{-1} \text{s}^{-1}$	[36]
D_e	0.015	$\text{m}^2 \text{s}^{-1}$	
D_l	2.5×10^{-6}	$\text{m}^2 \text{s}^{-1}$	
Γ_{T_l}	1×10^{10}	s^{-1}	[37]
Γ_{T_e}	1.2×10^{12}	s^{-1}	[37]
λ_{pump}	1500	nm	
K_e^{eq}	315	$\text{W m}^{-1} \text{K}^{-1}$	[34]
K_l^{eq}	2.5	$\text{W m}^{-1} \text{K}^{-1}$	[38]
$ \vec{E}_p $	10	MV/m	
l	20	nm	[2]

linearize Eqs. (3), namely,

$$T_e(\vec{r}, t) = T^{\text{eq}} + \delta T_e(\vec{r}, t), \quad \delta T_e \ll T^{\text{eq}} \quad (5a)$$

$$T_l(\vec{r}, t) = T^{\text{eq}} + \delta T_l(\vec{r}, t), \quad \delta T_l \ll T^{\text{eq}}. \quad (5b)$$

Moreover, Eq. (5) allows us to neglect the spatiotemporal dependence of the heat capacity and thermal conductivity so that

$$C_l \gg C_e^{\text{eq}} \gg \Delta C_e, \quad \delta K_{l,e} \ll K_{l,e}^{\text{eq}}. \quad (6)$$

Substitution of Eqs. (5) and (6) in Eq. (3) leads to the following system of equations

$$\frac{\partial \delta T_e}{\partial t} = D_e \nabla^2 \delta T_e - \Gamma_{T_e} (\delta T_e - \delta T_l) + f(\vec{r}, t), \quad (7a)$$

$$\frac{\partial \delta T_l}{\partial t} = D_l \nabla^2 \delta T_l + \Gamma_{T_l} (\delta T_e - \delta T_l), \quad (7b)$$

$$f(\vec{r}, t) \equiv \frac{P_{\text{abs}}(\vec{r}, t)}{C_e^{\text{eq}}}, \quad (7c)$$

where $\Gamma_{T_{e,l}}$ and $D_{e,l}$ represent the decay rates and diffusion coefficients of the electronic and lattice temperatures, respectively,

$$\Gamma_{T_e} \equiv \frac{G}{C_e^{\text{eq}}}, \quad D_e \equiv \frac{K_e^{\text{eq}}}{C_e^{\text{eq}}} \quad (8a)$$

$$\Gamma_{T_l} \equiv \frac{G}{C_l}, \quad D_l \equiv \frac{K_l^{\text{eq}}}{C_l}. \quad (8b)$$

Typical values of parameters used in the analytical solution of the linearized *TTM* (7) are given in Table I.

At this point, let us assume that the intensity profile is given according to Eq. (2) which for the chosen irradiation represents combinations of a constant ‘‘DC’’ term and a sum of two purely sinusoidal modulations modulated by exponential decay inside the bulk of the metal film. Since complex exponentials are eigenfunctions of the transverse part of the diffusion evolution operators in (7) we can expect that in the linear limit the periodic xy structure is exactly imprinted

also in the temperature variation albeit it is now time and z dependent.

It is convenient to define response functions $Z_{m,n}$ and $M_{m,n}$ of electron and lattice to the complex doubly-periodic Gaussian time-modulated excitation $f_{mn}(\vec{r}, t) = \exp(i 2\pi m x / \Lambda_x) \exp(i 2\pi n y / \Lambda_y) \exp(2z/l) \exp(-t^2/\tau_p^2) / \tau_p$ so that the corresponding solutions of (7) are given by $\tau_p Z_{mn}(z, t) \exp(i 2\pi m x / \Lambda_x) \exp(i 2\pi n y / \Lambda_y)$ and $\tau_p M_{mn}(z, t) \exp(i 2\pi m x / \Lambda_x) \exp(i 2\pi n y / \Lambda_y)$. These response functions for linearized system (7) can be found using standard Fourier expansion (see, e.g., Ref. [39]). The procedure is described in Appendix A and the results read:

$$Z_{mn}(z, t) = \frac{l l_{mn}}{2 D_e \tau_p} e^{z/l_{mn}} e^{-t^2/\tau_p^2}$$

$$M_{mn}(z, t) = \frac{l \Gamma_{T_l} e^{z/\tilde{l}_{mn}}}{2 \Gamma_{T_e} D_e |k_{\pm}|^2 \tau_p} \text{Re} \left[k_{\pm} e^{i \tilde{k}_0 z} \right. \\ \left. \times \left(e^{-(t/\tau_p)^2} + \frac{i \sqrt{\pi} \Gamma_{T_e} \tau_p}{2} (1 + \text{Erf}(t/\tau_p)) \right) \right]$$

$$l_{mn} = (k_{mn}^2 + \Gamma_{T_e}/D_e)^{-1/2},$$

$$k_{mn}^2 = \left(\frac{2\pi m}{\Lambda_x} \right)^2 + \left(\frac{2\pi n}{\Lambda_y} \right)^2 k_{\pm}^2 \\ = -i \sqrt{k_{mn}^2 + (\Gamma_{T_e}/D_e)(1 \pm i)}$$

$$= \pm \tilde{k}_0 - i/\tilde{l}_{mn}. \quad (9)$$

Using these notations the analytical solution of Eq. (5) for the variation of electronic temperature δT_e has the form:

$$\delta T_e(x, t) = \delta T_{\text{tot}} Z_{00}(z, t) + \delta T_x \cos \left[2\pi \frac{x}{\Lambda_x} + 2\phi_x \right] Z_{10}(z, t) \\ + \delta T_y \cos \left[2\pi \frac{y}{\Lambda_y} + 2\phi_y \right] Z_{01}(z, t), \quad (10)$$

where

$$\delta T_x = \frac{p_0 \alpha \tau_p}{2 C_e^{\text{eq}}}, \quad \delta T_y = \frac{p_0 \beta \tau_p}{2 C_e^{\text{eq}}} \quad (11)$$

$$\delta T_{\text{tot}} = \delta T_x + \delta T_y = \frac{p_0 \tau_p}{2 C_e^{\text{eq}}}. \quad (12)$$

The expression for the lattice temperature is obtained by replacing Z_{mn} functions with M_{mn} from Eq. (9).

A few remarks are in order. According to (9), (10) the temporal dynamics of the temperature excitation of the electron subsystem follows that of the pump pulse and is transient with the same timescale τ_p . This happens because the typical electron relaxation time $(\Gamma_{T_e} + D_e k_{mn}^2)^{-1}$ is much shorter than the pulse width—not least because of the large spatial bandwidth of the source in the z direction. Therefore the electron subsystem reacts almost instantaneously. The lattice response however is more complex. According to Eqs. (9) and (10) it is characterized by a fast transient phase (the first term in the expression for M_{mn}) followed by a long period of relaxation. In fact it follows from Eq. (9) that the lattice temperature excitation at a given point does not die down but tends to a constant limit, but a more careful analysis [see Eq. (A7)] shows that it does decay but at much larger timescales of the order of $\Gamma_{T_l}^{-1} \sim 100$ ps.

As for the spatial dependence one can see from (10) that each transverse spatial harmonic \vec{k}_{mn} from the dissipated energy density (2) is carried over to the corresponding harmonic of the temperature variation profile but modulated in time and depth z by the functions Z_{mn} and M_{mn} . Each of these functions decays in metal on the scale l_{mn} (electrons) and \tilde{l}_{mn} (lattice), both of which are k dependent and much larger than the skin depth l [40]. The “DC term” for example decays slowest with $l_{00} = 112$ nm (electrons) and $\tilde{l}_{00} = 101$ nm (lattice). Assuming $\lambda = 1.5$ μm and equal incidence angles $\theta_x = \theta_y = \pi/4$ the interference terms in (10) decay at the scale $l_{10} = l_{01} = 93$ nm (electrons) and $\tilde{l}_{10} = \tilde{l}_{01} = 88$ nm lattice. Notice however that both scales are larger than the skin depth l . In addition the lattice perturbation also experiences z oscillations on a scale \tilde{k}_0^{-1} comparable to the decay.

IV. SIMULATION RESULTS

In order to demonstrate the feasibility of the field-induced transient structures and compare them to the results of linear theory we have performed a series of numerical simulations of the master TTM model (3). We have picked equally balanced beams with $\alpha = \beta = 1/2$, $\phi_x = \phi_y = 0$, and $\theta_x = \theta_y = \pi/4$. The pulse duration was $\tau_p = 1$ ps and the initial conditions corresponded to the equilibrium temperature $T^{\text{eq}} = 300$ K.

In Fig. 2 we show the dependence of the maximum temperature [over time and the transverse plane (x, y)] as a function of the penetration depth z . Although the induced temperature change of the electron subsystem cannot be considered small one can observe qualitative agreement with the linear theory of the previous chapter. In particular the temperature perturbation decays at the typical scale $\tilde{l} \sim 100$ nm $\gg l$. Additionally the lattice temperature variations, while being small, display additional nonmonotonic behavior as predicted by the linear theory.

The full numerical simulations of 3 + 1 system (3) (three coordinates plus time) are quite time consuming. Therefore the following results represent simulation of z -averaged model which is effectively 2 + 1 dimensional and the resulting temperature distributions $T_{e,l}(x, y, t)$ are obtained by averaging over z interval of length $\tilde{l} = l_{00} \approx 100$ nm. This corresponds to considering only transverse coordinates in (3) and z averaging the exponentially decaying source term (2) which in turn corresponds to the renormalization of the peak power density $p_0 \rightarrow \tilde{p}_0 = p_0(l/2\tilde{l})[1 - \exp(-2\tilde{l}/l)] = 0.1 p_0$. This procedure is mathematically justified when the temperature deviations are small as in the previous section and the heat capacities/conductivities can be treated as constants. In the case of large deviation we still argue that the z averaging represents a qualitatively correct “mean-field” representation of the temperature distribution in the film.

In Fig. 3, we concentrate on the spatial periodicity of the structures. We have picked a time corresponding to maximum visibility for electron and lattice temperature lattices, respectively. For the electrons this corresponds to the temporal maximum of the irradiating pulse, i.e., $t = 0$ and for the lattice there is a delay in the dynamics and we have chosen the time corresponding to $\approx \tau_p$.

One can see that the doubly-periodic pattern of the irradiating cross beams is duly reproduced in the temperature

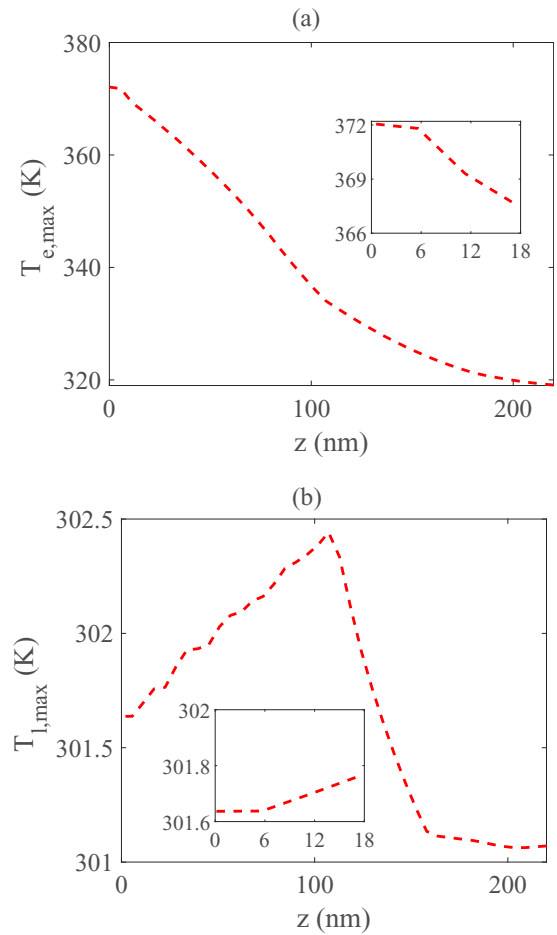


FIG. 2. Maximum temperature variation as a function of thickness of the metallic film when the absorbed power density is $p_0 \approx 2.4$ $\text{J cm}^{-3} \text{ps}^{-1}$. (a) Electronic temperature $T_{e,\text{max}}$ and (b) lattice temperature $T_{l,\text{max}}$. The insets show the boundary layer demonstrating vanishing flux.

distribution of both electron and lattice subsystems. The induced lattice temperature change is as expected much smaller and the theory overestimates the contrast somewhat. For the electrons the coincidence is almost perfect.

Next in order to demonstrate the transient nature of the structures we consider temporal dynamics of the temperature slices along the y axis ($x = 0$). The results are presented in Fig. 4 for the same parameters as in Fig. 3. One can clearly see the separation of the fast and slow relaxation rates of the temperature and lattice subsystems, respectively. In the following section we shall use the results for the depth-averaged temperature profile to demonstrate that they lead to the inscription of a transient 2D dissipative plasmonic crystal for the probe plasmon wave propagating at the metal-dielectric interface.

V. SPECTRAL PROPERTIES OF THE TRANSIENT DISSIPATIVE PLASMONIC CRYSTAL

The idea of using transient change of temperature induced by a pump wave to control dielectric constant for a probe wave propagating along the film or bulk material is not new

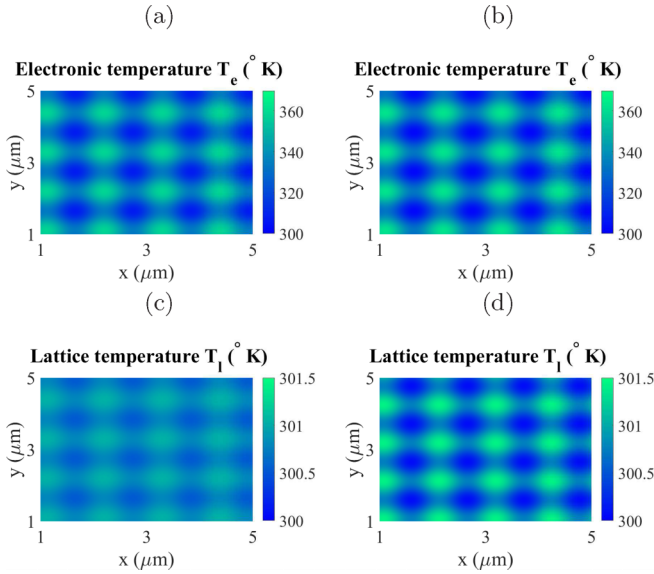


FIG. 3. The spatial profile of the induced temperature distribution. The magnitude of the z -averaged absorbed power density is $\bar{p}_0 = 2.4 \text{ J cm}^{-3} \text{ ps}^{-1}$. (Top) The “electron temperature crystal.” (Bottom) The “lattice temperature crystal.” (a), (c) full numerics; (b), (d) linear theory.

[22,24–27]. However to the best of our knowledge these studies concentrated on 1D Bragg gratings and no attempts were made to study the transmittance spectra of these structures in a systematic way. In this section we show that in the NIR the main temperature effect is in the transient modulation of the imaginary part of the dielectric function and we calculate the resonant transparency of the structure near the Bragg resonance.

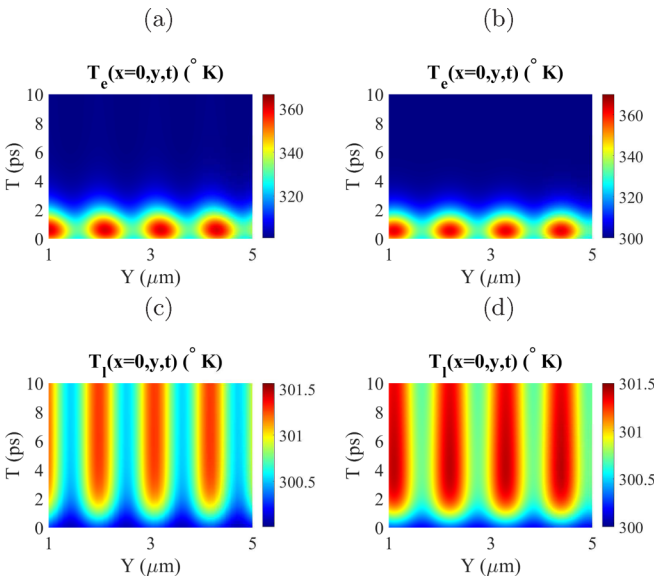


FIG. 4. The spatiotemporal evolution of the induced lattices along the y -axis direction. The field magnitude is the same as in Fig. 3. (Top) Electron temperature dynamics. (Bottom) Lattice temperature dynamic. (a), (c) full numerics; (b), (d) linear theory.

In order to translate the temperature change of both lattice and the electrons into the corresponding change of the complex dielectric constant of the metal film ε_m we assume here a simple Drude model model [2]:

$$\varepsilon_m = 1 - \frac{\omega_p^2}{\omega(\omega + i\gamma)} \quad (13a)$$

$$\omega_p = \frac{n_e e^2}{m_e \epsilon_0}, \quad (13b)$$

where the effect of the temperatures T_e and T_l is chiefly on the Umklapp electron-electron and electron-phonon scattering rates determining the imaginary part of the permittivity:

$$\gamma = \gamma_{e-e}^{\text{Um}}(T_e) + \gamma_{e-ph}(T_l) \quad (14a)$$

$$\gamma_{e-e} = A \Delta^{\text{Um}} T_e^2 \quad (14b)$$

$$\gamma_{e-ph} = B T_l. \quad (14c)$$

For Au, $A = 1.7 \times 10^7 \text{ K}^{-2} \text{ s}^{-1}$, $B = 1.45 \times 10^{11} \text{ K}^{-1} \text{ s}^{-1}$, and $\Delta^{\text{Um}} = 0.77$ [27]. Note that ω now refers to the frequency of a probe wave (SPP) propagating in the metal film with the modulated permittivity ε_m . Here we neglect the induced variation of the permittivity in the dielectric and assume $\varepsilon_d = \text{const}$.

Let us denote the scattering rate at equilibrium temperature T^{eq} as γ_0 . According to Eq. (14) one has for gold $\gamma_0 = 4.46 \times 10^{13} \text{ s}^{-1}$. We are interested in the regime of low losses when $\gamma_0 \ll \omega < \omega_p = 9 \text{ eV} \approx 1.37 \times 10^{16} \text{ s}^{-1}$. One can then expand the Drude formula (13) to yield:

$$\varepsilon_m \approx 1 - \frac{\omega_p^2}{\omega^2} + i \frac{\omega_p^2 \gamma}{\omega^2 \omega}.$$

The above result means that the spatiotemporal modulation of the lattice and electron temperatures translates into spatiotemporal modulation of the permittivity as attested by Fig. 5, where we plot the numerically obtained changes of the real and imaginary part of the metal permittivity. These were calculated at the frequency $\omega = \omega_{\text{SPP}} = 8.6 \times 10^{14} \text{ rad/s}$ which, as we shall see below, corresponds to the typical Bragg resonance frequency of the dynamical plasmonic structure. For both subsystems we have chosen a time moment corresponding to the maximum perturbation of the dielectric function and also picked a strong pulse in order to maximize the contrast—see below. According to the results of Sec. III and the simulations of Fig. 4 the excitations of the electron and lattice subsystems are well separated in time: By the time $\sim \tau_p$ that the lattice temperature begins to build up the electron temperature change has died out. This means that at each given moment only one scattering mechanism in (14) contributes to the Drude permittivity. Thus the maximum induced relative change of the real part of the refractive index $|\Delta \varepsilon' / \varepsilon_m'|$ is ≈ 0.032 for the electrons and 6×10^{-4} for the lattice, while the corresponding ratios for the imaginary part $|\Delta \varepsilon'' / \varepsilon_m''|$ are ≈ 1.5 for the electrons and 0.0346 for the lattice, respectively. From this we conclude that the main temperature effect on the electromagnetic properties of the film are in the periodic modulation of the losses and not in the band-gap opening characteristic of most SPC structures [3–5].

Linearizing the scattering rate $\gamma(T_e, T_l)$ around the equilibrium value we can assume that the temperature induced

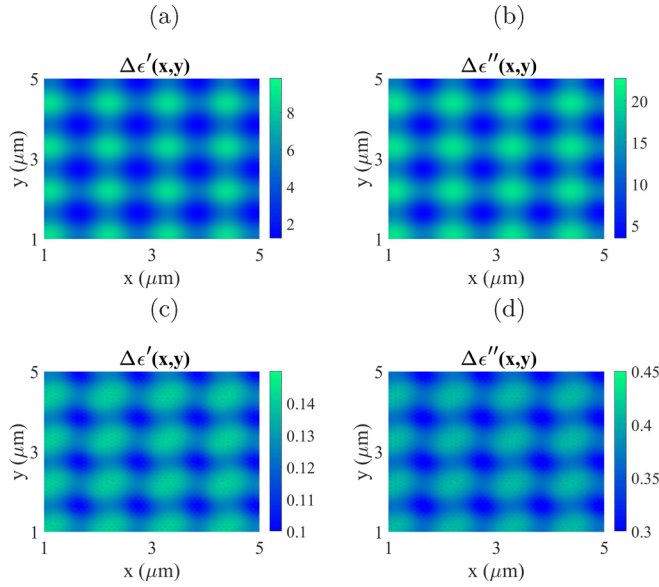


FIG. 5. The spatial profile of the variation of the dielectric function $\Delta\epsilon$ when the magnitude of the absorbed power density is $\bar{p}_0 = 22 \text{ J cm}^{-3} \text{ ps}^{-1}$. (Top) Electronic subsystem. (Bottom) Lattice subsystem. (a), (c) real part; (b), (d) imaginary part.

change of the imaginary part of permittivity is proportional to the sum of the changes induced by electron and lattice, respectively, since their temporal windows do not overlap (see Fig. 4). The electron-induced change is much stronger—Figs. 5(b) and 5(d)—but it is short lived on the scale of the pump pulse while the lattice induced change is significantly weaker but long lived as discussed in the previous section.

Let us assume for simplicity the symmetric irradiation with $\theta_x = \theta_y = \theta$, $\phi_{x,y} = 0$, $\alpha = \beta = 1/2$. Then one can describe the transient dissipative plasmonic crystal with the following model:

$$\begin{aligned} \epsilon_m(x, y; t) &= \epsilon'_m + i \epsilon''_m(x, y; t), \quad \epsilon'_m = 1 - \frac{\omega_p^2}{\omega^2} < 0 \\ \epsilon''_m(x, y; t) &= \Delta\epsilon''(t) \left[1 + s(t) \cos\left(\frac{2\pi x}{\Lambda}\right) \right. \\ &\quad \left. + s(t) \cos\left(\frac{2\pi y}{\Lambda}\right) \right] \end{aligned} \quad (15)$$

with new common period $\Lambda = \Lambda_x = \Lambda_y = \lambda/(2 \sin \theta)$. At each time moment we have defined the background $\Delta\epsilon''(t)$ and the contrast $s(t)$. In the weak perturbation limit both values can be easily calculated via Eq. (10).

From the results observed in Fig. 5 one can see that the spatial dependence can be fitted by the model (15) where the background and the contrast can be extracted from the simulation data via:

$$\begin{aligned} \Delta\epsilon''(t) &= \frac{\max_{x,y} \epsilon''_m(x, y; t) + \min_{x,y} \epsilon''_m(x, y; t)}{2} \\ 2s(t) &= \frac{\max_{x,y} \epsilon''_m(x, y; t) - \min_{x,y} \epsilon''_m(x, y; t)}{\max_{x,y} \epsilon''_m(x, y; t) + \min_{x,y} \epsilon''_m(x, y; t)}. \end{aligned}$$

Assuming the constant positive relative permittivity ϵ_d in the dielectric $z > 0$ and slowly varying complex periodic $\epsilon_m(x, y; t)$ given by Eq. (15) in metal $z < 0$ we can seek

the solution of Maxwell's equation for the probe field in the slowly-varying envelope (SVE) approximation: $\vec{E} = \vec{E}(x, y, z; t) e^{-i\omega t}$, $\vec{H} = \vec{H}(x, y, z; t) e^{-i\omega t}$ where the envelope functions vary on timescales similar to the dielectric permittivity, i.e., $\tau_e \sim \tau_p$ or $\tau_l \gg \tau_p$ which are assumed to be much longer than the period of the mode $2\pi/\omega$. For example, for 1 ps pump pulse this allows us to use SVE for probe wavelengths up to a millimeter range.

From now on we can drop time dependence assuming that we are considering the crystal properties at a prescribed time moment. The analytical study of PCs with sinusoidal modulation of permittivity was performed by Darmanyan and Zayats [5] for the static structures in the conservative case when no scattering losses were taken into account ($\gamma = 0$) and only the real part of ϵ_m was modulated. They obtained the expression for the band-gap opening of the structure. Here we follow a similar approach but for the dissipative modulation and demonstrate enhanced transmittance at the Bragg resonance, i.e., the opposite of the forbidden zone. In what follows we shall concentrate on the fast electron-induced modulation of losses as the lattice effects are at least an order of magnitude weaker.

In the absence of dissipative spatial modulation the dielectric function $\epsilon(z) = \epsilon'(z)$ is real piecewise constant and Maxwell's equation admits surface plasmon-polariton (SPP) solutions which for the x -traveling modes ($k_y = 0$) take the form [2]:

$$\begin{aligned} \vec{H} &= A(0, 1, 0) e^{i k_x x + i k_z(z) z} = \vec{H}(z) e^{i k_x x} \\ \vec{E} &= \frac{A}{\omega \epsilon_0 \epsilon(z)} (k_z(z), 0, -k_x) e^{i k_x x + i k_z(z) z} = \vec{E}(z) e^{i k_x x} \\ k_z(z) &= i \text{Sign}[z] \sqrt{k_x^2 - k_0^2 \epsilon(z)}, \quad k_0 = \omega/c \\ k_x &= k_0 \sqrt{\frac{\epsilon_d \epsilon'_m}{\epsilon_d + \epsilon'_m}}, \quad k_x \geq k_0 \sqrt{\epsilon_d}. \end{aligned} \quad (16)$$

Here, we assume that the localization length in metal is much less than the width of the film and the effects of the substrate can be neglected. The amplitude A is related to the power modal density [9,41]:

$$P = \frac{1}{2} \int dy \int dz \vec{E} \times \vec{H}^* \cdot \vec{e}_x = \frac{k_x W |A|^2 \epsilon'_m |k_z^m| + \epsilon_d |k_z^d|}{\omega \epsilon_0 2 \epsilon_d \epsilon'_m |k_z^d| |k_z^m|},$$

where W is the width of the sample in the y direction, $k_z^d = k_z(z > 0)$, $k_z^m = k_z(z < 0)$.

By periodic modulation of the real part of the permittivity a SPC can be created whereas the continuous dispersion law of SPP given by the last Eq. (16) folds into a series of Floquet-Bloch bands inside the first 2D Brillouin zone (BZ) separated by band gaps [3–5]. A gap in the m th band opens at the border of the BZ where an SPP propagating in a direction of, say, x axis with the wave vector k_x is in Bragg resonance with the backscattered SPP so that one has $k_x \approx -k_x + 2\pi m/\Lambda$. In our case, however, the temperature induced grating modulates predominantly the imaginary part of permittivity and the Bragg resonance leads to a different type of phenomena as discussed below. It is important to note that the boundary of the BZ given by $k_G = \pi/\Lambda$ occurs at relatively low frequencies. Indeed assuming the wavelength $\lambda_p = 1.55 \mu\text{m}$ for the

pump wave and $\theta = \pi/4$ one has $k_G = 2.86 \times 10^6 \text{ m}^{-1}$ which according to dispersion law for SPP (16) (assuming air for the covering dielectric) corresponds to the SPP frequency of $\omega = 0.06 \omega_p = 8.6 \times 10^{14} \text{ rad/s}$ (which is still much greater than the scattering loss γ_0).

The full analysis of the transmittance of the dissipative SPC requires full simulation using either Green function formalism or plane wave expansion [4]. But in order to give a qualitative description of the effect we opt for a much simpler, semianalytical approach relying on the coupled mode theory. This approach is similar to that considered, e.g., in Refs. [5,9]. We consider coupling of only two SPPs propagating in the opposite directions of the x axis with the propagation constants $\pm k_x$ close to resonance so that $-k_x \approx k_x - 2\pi/\Lambda$. Note that for purely sinusoidal coupling (15) the Bragg resonance only occurs in the first band $m = 1$.

Introducing the forward and backward traveling waves with slowly varying amplitudes $c_{\pm}(x) \exp(\pm i k_x x)$ the standard coupled mode theory [9,41] leads to the following system of equations:

$$\begin{aligned} \frac{dc^+}{dx} &= K^{+,+}(x) c^+(x) + K^{+,-}(x) c^-(x) e^{-2i k_x x} \\ \frac{dc^-}{dx} &= K^{-,+}(x) c^+(x) e^{2i k_x x} + K^{-,-}(x) c^-(x) \\ K^{p,q} &= pK^z(x) + qK^x(x), \quad p, q = \pm \\ K^x(x) &= \frac{i \omega \varepsilon_0}{4P} \int dy \int_{z < 0} dz i \varepsilon_m''(x, y) |\mathcal{E}_x(z)|^2 \\ &= -\frac{1}{4} \frac{\varepsilon_d |k_z^d| |k_z^m|^2 \Delta \varepsilon''}{k_x \varepsilon_m' (\varepsilon_d |k_z^d| + \varepsilon_m' |k_z^m|)} \left[1 + s \cos\left(\frac{2\pi x}{\Lambda}\right) \right] \\ &= -\bar{K} \left[1 + s \cos\left(\frac{2\pi x}{\Lambda}\right) \right] K^z(x) \\ &= \frac{i \omega \varepsilon_0}{4P} \int dy \int_{z < 0} dz i \varepsilon_m''(x, y) |\mathcal{E}_z(z)|^2 \\ &= \left(\frac{k_x}{|k_z^m|} \right)^2 K^x(x), \end{aligned} \quad (17)$$

where we have neglected the coupling to the nonresonant modes.

Near the resonance one has $\omega \ll \omega_p$ and $k_x \approx k_0 \sqrt{\varepsilon_d}$ so that $(k_x/|k_z^m|)^2 \approx \varepsilon_d/|\varepsilon_m'| \ll 1$ and one can write approximately $\bar{K} \approx k_0 \varepsilon_d^{3/2} \Delta \varepsilon''/4 |\varepsilon_m'|^2$ with the longitudinal coupling $K^x(x)$ dominating over the transverse one. Introducing the small detuning from the Bragg resonance $\delta = k_x - \pi/\Lambda$ and keeping only the resonant terms in (17) one obtains

$$\begin{aligned} \frac{dc^+}{dx} &= -\bar{K} c^+ + \frac{\bar{K} s}{2} e^{-2i\delta x} c^- \\ \frac{dc^-}{dx} &= -\frac{\bar{K} s}{2} e^{2i\delta x} c^+ + \bar{K} c^- \end{aligned}$$

to be solved with the boundary conditions $c^+(0) = 1$, $c^-(L) = 0$ where L is the length of the grating. When no modulation is present, $s = 0$, one expects exponential decay of transmittance according to the Beer law: $T_0 = |c^+(L)|^2 = \exp(-2\bar{K}L)$. The resonant coupling leads to the

power exchange between the forward (pump) and the backward (Stokes) waves with the latter partially offsetting the loss in the former.

A straightforward calculation yields the expression for the transmission and the reflection coefficients as the functions of modulation depth s at a given frequency:

$$\begin{aligned} \mathcal{T}(s; \delta) &= |c^+(L)|^2 = |\cosh(\Delta L) + (\bar{K} - i\delta) \sinh(\Delta L)/\Delta|^{-2} \\ \mathcal{R}(s; \delta) &= |c^-(0)|^2 = \frac{s^2 \bar{K}^2}{4} |\bar{K} - i\delta + \Delta \coth(\Delta L)|^{-2} \\ \Delta &= \bar{K} \sqrt{(1 - i\delta/\bar{K})^2 - s^2/4}. \end{aligned}$$

This result was obtained earlier in Ref. [30] in the context of sound waves in porous media [42]. Both functions are symmetric and reach maximum value at the resonance $\delta = 0$. The characteristic decay length at zero contrast is given by $1/(2\bar{K})$. At large values of $\bar{K}L$ the transmission at resonance $\delta = 0$ follows Beer law, namely $T \propto \exp(-\alpha L)$ where the attenuation coefficient is given by:

$$\alpha = L'^{-1} = 2\bar{K} \sqrt{1 - s^2/4}. \quad (18)$$

Recall now that all the quantities s and L' are dynamic variables changing on the scale of the incident pulse τ_p . Both are plotted as function of time in Fig. 6. Note the transient character of both $s(t)$ and $L'(t)$. At the very large power density of the pump the contrast does not wash out completely but decays slowly well after the transit of the pump pulse. This is due to the fact that at such high energies the induced lattice temperatures become significant and as discussed in the previous section it is characterized by much slower dynamics. Technically however at such large energies and temperature changes the linearization approach of Sec. III and the linearized model (15) are no longer valid so the red curves are given for reference only.

Note also that unlike the case of real modulation of the dielectric permittivity that opens a band gap at the Bragg resonance the purely dissipative modulation increases the transmission at the resonance compared to the unmodulated case $s = 0$. This enhancement is more pronounced for larger propagation distances when $L \gg L'$ and in this regime is given by:

$$\frac{T_{\max}(s)}{T_0} = 4 \frac{4 - s^2}{(2 + \sqrt{4 - s^2})^2} e^{\bar{K}L(2 - \sqrt{4 - s^2})}.$$

This effect is illustrated for both transmission and reflection in Fig. 7 for $\bar{K}L = 10$. Its physical explanation is simple and goes beyond the applicability of the coupled mode theory [30]. When the period of the imaginary part of the permittivity modulation is equal to the spacial period of the SPP in (16) the resulting field pattern forms a standing wave where the nodes are at the position of maximum values of the imaginary part of the permittivity while the maxima of the wave coincide in with the minima of the loss. Thus the SPP can adjust itself to minimize the absorption compared to the unmodulated structure and thanks to this effect increase both the transmission and the reflection.

Finally, let us notice a curious possibility of a ‘‘phase transition’’ occurring in the structure at $s = s_* = 2$. Indeed,

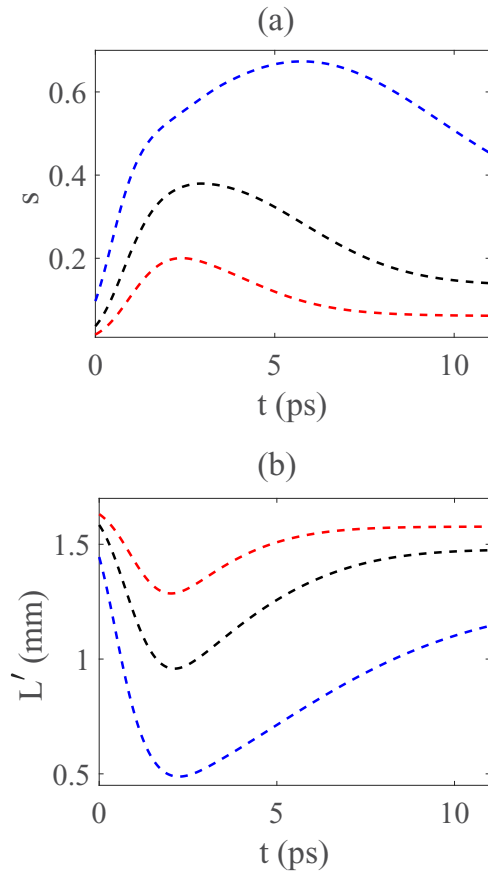


FIG. 6. Temporal dependence of the (a) contrast s and (b) characteristic decay length L' (18). Black blue and red dash-dotted curves correspond to the magnitude of absorbed power density $\bar{p}_0 = 11, 22, 63 \text{ J cm}^{-3} \text{ ps}^{-1}$, respectively.

at the resonance $\delta = 0$ the eigenvalues of the matrix in the r.h.s. of the coupled mode equations $\lambda_{\pm} = \pm\sqrt{1 - s^2/4}$ become imaginary and the transmittance no longer decays exponentially but oscillates with the length of the structure. There is nothing particularly surprising in this behavior as according to the model (15) already for $s \geq 1/2$ the induced grating ceases to be purely passive (ϵ_m'' makes excursions into negative values), and thus attenuation is no longer necessarily a dominating mode of operation. As one can see from Fig. 6 even for the very intensive pulses at the boundary of the applicability of the linearized theory the contrast does not quite reach such levels however the transition can be potentially observed by shifting the irradiating wavelengths from infrared to visible light thus increasing the resonance frequency.

Finally let us discuss applicability of the results of this section. Firstly the z -averaged model is inapplicable if the probe plasmon penetration depth in metal becomes larger than the lattice depth $\tilde{l} \sim l_{00} \sim 100 \text{ nm}$. Near the Bragg resonance the former can be estimated as $l_z \sim |k_z|^{-1} \sim 1/(|\epsilon_m'|^{1/2} k_0) \sim 20 \text{ nm}$. Therefore the probe plasmon does indeed see a uniform lattice and our approximation is self-consistent. Next, the large contrast s as discussed above requires large temperature perturbations that lead to the appearance of higher spatial harmonics in the dielectric function (15). These har-

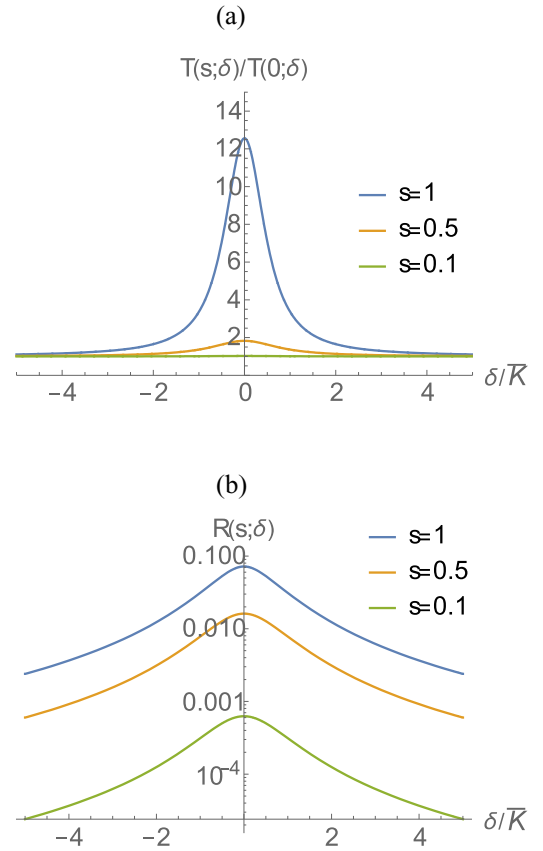


FIG. 7. (a) The maximum value of resonant transmittance of the transient PC for several values of the contrast parameter s . (b) The reflectivity of the same structure.

monics should open additional higher order resonances as well as modulate the real part of ϵ thus leading to the potential opening of the transient band-gap structure [3]. However we leave the analysis of these phenomena for the future studies.

VI. DISCUSSION

In this paper, we have shown that by exciting electron and lattice subsystems of a metal film by a system of orthogonal overlapping pulses of given period one can inscribe a transient SPC. The electron subsystem responds more strongly but decays on the time scale of the pulse (picoseconds) while the lattice-induced changes are long lived but produced negligible contrast. The depth of the inscribed lattice was found to be much larger than the skin depth of the pump beam provided that the film is thick enough ($> 100 \text{ nm}$), and the effects of the substrate can be ignored.

In the NIR, the induced lattice provides a Bragg resonance for a probe SPP field in the same spectral area which is far below the plasma frequency and therefore can only couple SPPs that are not localized in the dielectric cover. In this regime, the Drude mechanism imposes periodic modulation of the imaginary part of the dielectric function and we do not expect a significant band-gap opening in this situation. Instead we have studied the effects of resonant transparency

of the structure within the framework of the coupled mode theory.

There are multiple avenues open for further study of these structures. In particular, it is desirable to provide an efficient coupling mechanism in the visible part of the spectrum which requires increasing the boundary of the BZ and moving the frequencies of the irradiating pulses to the visible area accordingly. However at the visible range, e.g., for gold a simple Drude model (13) for the dielectric function is no longer adequate and one needs to include the interband transitions. This will require performing *ab initio* calculations of the interband transition which is a challenging task—see, e.g., Refs. [43,44]. This, however, is an interesting direction as potentially it may allow one not only to couple truly localized SPPs but also according to the result of our coupled mode analysis can make the structure transparent at given time marks provided that the induced contrast $s(t)$ is greater than the critical value $s_* = 2$. In the visible regime one can also hope to create a sizable band-gap opening due to increased magnitude of the real part of the induced change of the dielectric function thus paving the way to hybrid active-passive SPC and transient PT-symmetric structures [45].

APPENDIX: THE SOLUTION OF THE LINEARIZED TTM

In the Fourier domain system (7) becomes a system of linearly coupled ODE and its formal solution with vanishing normal component of the heat flux at the metal-dielectric interface $z = 0$ is given by:

$$\begin{aligned} \begin{pmatrix} \delta T_e(\vec{r}, t) \\ \delta T_l(\vec{r}, t) \end{pmatrix} &= \int d\vec{k}_\perp e^{i\vec{k}_\perp \cdot \vec{\rho}} \int_{-\infty}^0 dk_z \cos(k_z z) \\ &\times \int_{-\infty}^t dt' e^{\hat{A}(t-t')} \tilde{f}(\vec{k}, t') \begin{pmatrix} 1 \\ 0 \end{pmatrix} \\ \hat{A} &= \begin{pmatrix} -D_e k^2 - \Gamma_{T_e} & \Gamma_{T_e} \\ \Gamma_{T_l} & -D_l k^2 - \Gamma_{T_l} \end{pmatrix} \\ \tilde{f}(\vec{k}, t) &= \frac{1}{(2\pi)^2} \frac{2}{\pi} \int_{-\infty}^0 dz \cos(k_z z) \\ &\times \int f(\vec{r}, t) e^{-i\vec{k}_\perp \cdot \vec{\rho}} d\vec{\rho}, \end{aligned} \quad (\text{A1})$$

where $\vec{\rho} = (x, y, 0)$, $\vec{k}_\perp = (k_x, k_y, 0)$, $k^2 = k_\perp^2 + k_z^2$.

The evaluation of matrix exponential is straightforward but the resulting expressions for the matrix elements are rather cumbersome. The calculation can be significantly simplified if we note that according to Eq. (2) for the dissipated field the transverse Fourier transform of the source f contains apart from a DC term the harmonics at spatial frequencies $k_\perp^{\max} = 2\pi/\Lambda_{x,y} < 4\pi/\lambda$. On the other hand the sine transform of the exponentially decaying field intensity $\sim \exp(-2z/l)$ is proportional to the Lorentzian $(1 + (k_z l)^2/4)^{-1}$. The normal frequency cutoff is therefore $k_z^{\max} \sim l^{-1} \gg k_\perp^{\max}$. Then from Table I we see that $D_e(k_z^{\max})^2 \gg D_e(k_\perp^{\max})^2 \sim \Gamma_{T_e} \gg \Gamma_{T_l} \gtrsim D_l(k_z^{\max})^2$. Therefore we conclude that the lattice diffusion D_l can always be safely neglected while the lattice decay Γ_{T_l} can

be treated perturbatively compared to the electron diffusion and coupling.

We can introduce the characteristic diffusion damping according to the definition $\Gamma_{\text{diff}}(k) = D_e k^2 = D_e(k_z^2 + k_\perp^2)$. In the absence of coupling and electron decay $\Gamma_{\text{diff}}^{-1}(k)$ has the physical meaning of typical diffusion-induced decay for a sinusoidal source with the wave vector \vec{k} .

Then to the first order of the perturbation theory the eigenvalues and eigenvectors of matrix \hat{A} are given by

$$\begin{aligned} \lambda_e(k) &= -\Gamma_{T_e} - \Gamma_{\text{diff}}(k), \\ |e\rangle &= \begin{pmatrix} 1 \\ 0 \end{pmatrix} - \frac{\Gamma_{T_l}}{(\Gamma_{\text{diff}}(k) + \Gamma_{T_e})^2 + \Gamma_{T_e}^2} \begin{pmatrix} \Gamma_{T_e} \\ \Gamma_{\text{diff}}(k) + \Gamma_{T_e} \end{pmatrix} \\ \lambda_l(k) &= -\Gamma_{T_l} \frac{\Gamma_{\text{diff}}(k) (\Gamma_{\text{diff}}(k) + \Gamma_{T_e})}{(\Gamma_{\text{diff}}(k) + \Gamma_{T_e})^2 + \Gamma_{T_e}^2}, \\ |l\rangle &= \frac{1}{\sqrt{(\Gamma_{\text{diff}}(k) + \Gamma_{T_e})^2 + \Gamma_{T_e}^2}} \begin{pmatrix} \Gamma_{T_e} \\ \Gamma_{\text{diff}}(k) + \Gamma_{T_e} \end{pmatrix}. \end{aligned}$$

The matrix exponential can be evaluated in the main order in Γ_{T_l} leading to the following solution:

$$\begin{aligned} \delta T_e(\vec{r}, t) &= \int_{-\infty}^0 dk_z \cos(k_z z) \int d\vec{k}_\perp e^{i\vec{k}_\perp \cdot \vec{\rho}} \\ &\times \int_{-\infty}^t dt' e^{\lambda_e(k)(t-t')} \tilde{f}(\vec{k}, t') \\ \delta T_l(\vec{r}, t) &= - \int_{-\infty}^0 dk_z \cos(k_z z) \int d\vec{k}_\perp e^{i\vec{k}_\perp \cdot \vec{\rho}} \frac{\lambda_l(k)}{\Gamma_{\text{diff}}(k)} \\ &\times \int_{-\infty}^t dt' [e^{\lambda_l(k)(t-t')} - e^{\lambda_e(k)(t-t')}] \tilde{f}(\vec{k}, t'). \end{aligned} \quad (\text{A2})$$

The response functions Z_{mn} and M_{mn} correspond to the source term in the form:

$$\begin{aligned} \tilde{f}(\vec{k}, t) &= \tau_p^{-1} \exp(-t^2/\tau_p^2) \delta(\vec{k}_\perp - \vec{k}_{mn}) \tilde{f}_{||}(k_z), \\ \vec{k}_{mn} &= (2\pi m/\Lambda_x, 2\pi n/\Lambda_y, 0) \\ \tilde{f}_{||}(k_z) &= \frac{l}{\pi} \frac{1}{1 + (k_z l)^2/4}. \end{aligned}$$

Then performing (trivial) integration over \vec{k}_\perp and over time from (A2) we obtain:

$$\begin{aligned} Z_{mn}(z, t) &= \tau_p^{-1} \int_{-\infty}^0 dk_z \cos(k_z z) G(\tau, \lambda_e(k) \tau_p) \tilde{f}_{||}(k_z) \\ M_{mn}(z, t) &= -\tau_p^{-1} \int_{-\infty}^0 dk_z \cos(k_z z) \frac{\lambda_l(k)}{\Gamma_{\text{diff}}(k)} \\ &\times [G(\tau, \lambda_e(k) \tau_p) - G(\tau, \lambda_l(k) \tau_p)] \tilde{f}_{||}(k_z), \end{aligned} \quad (\text{A3})$$

where $\tau = t/\tau_p$, $k = \sqrt{k_z^2 + k_{mn}^2}$ and the time-response kernel is defined as

$$G(\tau, \xi) = \frac{\tau_p \sqrt{\pi}}{2} e^{\xi \tau} e^{\xi^2/4} [1 + \text{Erf}(\tau + \xi/2)]. \quad (\text{A4})$$

For the electron response function for pulse duration of 1 ps and longer it follows that $|\xi| = |\lambda_e| \tau_p \gtrsim \Gamma_{Te} \tau_p = 1.2$. In practice due to the contribution of the normal component of the wave vector k_z one has $|\xi| \gg 1$ and we can obtain a much-simpler asymptote

$$G(t, \lambda_e(k) \tau_p) \approx -\frac{1}{\lambda_e(k)} e^{-(t/\tau_p)^2}, \quad t \lesssim |\xi| \tau_p, \quad (\text{A5})$$

which means that time response is almost instantaneous. With this simplification the integral over normal wave vector k_z can be calculated analytically yielding:

$$Z_{mn}(z, t) = \frac{\exp(-t^2/\tau_p^2)}{\tau_p(\Gamma_{mn} - 4\Gamma_{||})} \left[e^{2z/l} - 2\sqrt{\frac{\Gamma_{||}}{\Gamma_{mn}}} e^{\sqrt{\Gamma_{mn}/\Gamma_{||}} z/l} \right],$$

$$\Gamma_{||} = D_e/l^2$$

$$\Gamma_{mn} = \Gamma_{Te} + D_e k_{mn}^2. \quad (\text{A6})$$

One can see that the electron response has two components: the fast decaying one that does not penetrate more than one skin depth and a much longer one decaying on a scale $l_{m,n} =$

$(k_{mn}^2 + \Gamma_{Te}/D_e)^{-1/2}$. Moreover, from Table I and for low spatial harmonics $m, n \sim 1$ it follows that the ratio $\Gamma_{||}/\Gamma_{mn} \gg 1$ so that the long-scale contribution to $Z_{mn}(z)$ is dominating leading to the first equation in (9).

Let us now turn to the lattice response. The first term in the integral in (A3) can be again approximated as (A5). As for the second term, the argument $|\xi| = |\lambda_l| \tau_p \sim \Gamma_{Ti} \tau_p \sim 10^{-2} \ll 1$. Therefore the time kernel can be approximated as:

$$G(t, \lambda_l(k) \tau_p) = \frac{\tau_p \sqrt{\pi}}{2} e^{\lambda_l(k)t} [1 + \text{Erf}(t/\tau_p)]. \quad (\text{A7})$$

Up to typical times of the order $\Gamma_{Ti}^{-1} \sim 100 \text{ ps} \gg \tau_p$ the exponential can be put to unity. Then performing the integration over the transverse wave vector in (A3) we can close the contour in the lower complex plane and observe that the pole at $k_z = -2i/l$ leads to fast decaying terms with z similar to the electron subsystem. The magnitude of the prefactor of this term is of the order of $\Gamma_{Ti}/(\tau_p \Gamma_{mn} \Gamma_{||})$ and can be neglected. The other two contributing poles are located at $k_z = k_{\pm} = -i \sqrt{k_{mn}^2 + (\Gamma_{Te}/D_e)(1 \pm i)} = \pm \tilde{k}_0 - i/\tilde{l}_{mn}$ —the points where λ_l has poles. The contribution of these poles leads to the result (9) of the main text.

-
- [1] J. Joannopoulos, S. Johnson, J. Winn, and R. Meade, *Photonic Crystals – Molding the Flow of Light*, 2nd ed. (Princeton University Press, Princeton and Oxford, 2008).
- [2] S. Maier, *Plasmonics: Fundamentals and Applications*, 2nd ed. (Springer Science & Business Media, New York, 2007).
- [3] A. Zayats, I. Smolyaninov, and A. Maradudin, Nano-optics of surface plasmon polaritons, *Phys. Rep.* **408**, 131 (2005).
- [4] W. Dickson, G. Wurtz, and A. Zayats, in *Photonics: Scientific Foundations, Technology and Applications*, edited by D. Andrews (Wiley, Hoboken, NJ, 2015), Vol. 3, pp. 107–167.
- [5] S. A. Darmanyan and A. V. Zayats, Light tunneling via resonant surface plasmon polariton states and the enhanced transmission of periodically nanostructured metal films: An analytical study, *Phys. Rev. B* **67**, 035424 (2003).
- [6] L. Feng, M. Lu, V. Lomakin, and Y. Fainman, Plasmonic photonic crystal with a complete band gap for surface plasmon polariton waves, *Appl. Phys. Lett.* **93**, 231105 (2008).
- [7] M. P. van Exter, V. T. Tenner, F. van Beijnum, M. J. A. de Dood, P. J. van Veldhoven, E. J. Geluk, and G. W. 't Hooft, Surface plasmon dispersion in metal hole array lasers, *Opt. Express* **21**, 27422 (2013).
- [8] W. L. Barnes, T. W. Preist, S. C. Kitson, and J. R. Sambles, Physical origin of photonic energy gaps in the propagation of surface plasmons on gratings, *Phys. Rev. B* **54**, 6227 (1996).
- [9] A. J. Chaves and N. Peres, Propagation of surface plasmons on plasmonic bragg gratings, *J. Appl. Phys.* **125**, 243106 (2019).
- [10] D. von der Linde, K. Sokolowski-Tinten, and J. Bialkowski, Laser-solid interaction in the femtosecond time regime, *Appl. Surf. Sci.* **109**, 1 (1997).
- [11] X. Ni, C. Wang, L. Yang, J. Li, L. Chai, W. Jia, R. Zhang, and Z. Zhang, Parametric study on femtosecond laser pulse ablation of au films, *Appl. Surf. Sci.* **253**, 1616 (2006).
- [12] W. Cai, A. Libertun, and R. Piestun, Polarization selective computer-generated holograms realized in glass by femtosecond laser induced nanogratings, *Opt. Express* **14**, 3785 (2006).
- [13] A. Block, M. Liebel, R. Yu, M. Spector, Y. Sivan, F. J. G. de Abajo, and N. F. van Hulst, Tracking ultrafast hot-electron diffusion in space and time by ultrafast thermomodulation microscopy, *Sci. Adv.* **5**, eaav8965 (2019).
- [14] S. Anisimov, B. Kapeilovich, and T. Perelman, Electron emission from metal surfaces exposed to ultrashort laser pulses, *Sov. Phys. JETP* **39**, 375 (1974).
- [15] C. Kern, M. Zürch, and C. Spielmann, Limitations of extreme nonlinear ultrafast nanophotonics, *Nanophotonics* **4**, 303 (2015).
- [16] G. D. Tsibidis, M. Barberoglou, P. A. Loukakos, E. Stratakis, and C. Fotakis, Dynamics of ripple formation on silicon surfaces by ultrashort laser pulses in subablation conditions, *Phys. Rev. B* **86**, 115316 (2012).
- [17] G. Tsibidis, E. Skoulas, and E. Stratakis, Ripple formation on nickel irradiated with radially polarized femtosecond beams, *Opt. Lett.* **40**, 5172 (2015).
- [18] G. D. Tsibidis, E. Skoulas, A. Papadopoulos, and E. Stratakis, Convection roll-driven generation of supra-wavelength periodic surface structures on dielectrics upon irradiation with femtosecond pulsed lasers, *Phys. Rev. B* **94**, 081305(R) (2016).
- [19] E. Petrakakis, G. D. Tsibidis, and E. Stratakis, Modelling of the ultrafast dynamics and surface plasmon properties of silicon upon irradiation with mid-IR femtosecond laser pulses, *Phys. Rev. B* **99**, 195201 (2019).
- [20] R. W. Schoenlein, W. Z. Lin, J. G. Fujimoto, and G. L. Eesley, Femtosecond Studies of Nonequilibrium Electronic Processes in Metals, *Phys. Rev. Lett.* **58**, 1680 (1987).
- [21] M. Bonn, D. N. Denzler, S. Funk, M. Wolf, S. Svante Wellershoff, and J. Hohlfeld, Ultrafast electron dynamics at metal surfaces: Competition between electron-phonon coupling and hot-electron transport, *Phys. Rev. B* **61**, 1101 (2000).
- [22] Y. Takata, H. Haneda, T. Mitsuhashi, and Y. Wada, Evaluation of thermal diffusivity for thin gold films using femtosecond

- laser excitation technique, *Appl. Surf. Sci.* **189**, 227 (2002).
- [23] F. Masia, W. Langbein, and P. Borri, Measurement of the dynamics of plasmons inside individual gold nanoparticles using a femtosecond phase-resolved microscope, *Phys. Rev. B* **85**, 235403 (2012).
- [24] O. Käding, H. Skurk, A. A. Maznev, and E. Matthias, Transient thermal gratings at surfaces for thermal characterization of bulk materials and thin films, *Appl. Phys. A* **61**, 253 (1995).
- [25] K. Katayama, T. Sawada, Q. Shen, and A. Harata, Detection of photoinduced electronic, thermal, and acoustic dynamics of gold film using a transient reflecting grating method under three types of surface plasmon resonance conditions, *Phys. Rev. B* **58**, 8428 (1998).
- [26] A. Maznev, J. Johnson, and K. Nelson, Non-equilibrium transient thermal grating relaxation in metal, *J. Appl. Phys.* **109**, 073517 (2011).
- [27] Y. Sivan and M. Spector, Ultrafast dynamics of optically-induced heat gratings in metals, *ACS Photon.* **5**, 1271 (2020).
- [28] Y. Sivan, G. Ctistis, E. Yüce, and A. Mosk, Femtosecond-scale switching based on excited free-carriers, *Opt. Express* **23**, 16416 (2015).
- [29] L. Nicholls, T. Stefaniuk, M. Nasir, F. Rodríguez-Fortuño, G. A. Wurtz, and A. V. Zayats, Designer photonic dynamics by using non-uniform electron temperature distribution for on-demand all-optical switching times, *Nat. Commun.* **10**, 12967 (2019).
- [30] A. Cebrecos, R. Pico, V. Romero-Garcia, A. Yasser, L. Maigyte, R. Herrero, M. Botey, V. J. Sánchez-Morcillo, and K. Staliunas, Enhanced transmission band in periodic media with loss modulation, *Appl. Phys. Lett.* **105**, 204104 (2014).
- [31] E. Lifshitz and L. Pitaevskii, *Electrodynamics of Continuous Media*, 5th ed. (Fizmatlit, Moscow, 2001).
- [32] H. Liu, J. Peng, W. Liu, Y. Wang, J. Wu, G. Zhang, X. Wang, and Y. Yan, Strong interference-based ultrathin conductive anti-reflection coating on metal substrates for optoelectronics, *NPG Asia Mater* **10**, 309 (2018).
- [33] In general, the lattice heat capacity C_l depends on the lattice temperature T_l through the Debye model [34]. However, in the current temperature range, $T_l \gtrsim T_D$, we can neglect its temperature dependence.
- [34] N. W. Ashcroft and N. D. Mermin, *Solid State Physics* (Saunders College, Philadelphia, 1976).
- [35] L. Jiang and H. Tsai, Improved two-temperature model and its application in ultrashort laser heating of metal films, *J. Heat Transfer* **127**, 1167 (2005).
- [36] P. Allen, Theory of Thermal Relaxation of Electrons in Metals, *Phys. Rev. Lett.* **59**, 1460 (1987).
- [37] C. K. Sun, F. Vallee, L. Acioli, E. P. Ippen, and J. G. Fujimoto, Femtosecond tunable measurement of electron thermalization in gold, *Phys. Rev. B* **48**, 12365 (1993).
- [38] Y. Wang, Z. Lu, and X. Ruan, First principles calculation of lattice thermal conductivity of metals considering phonon-phonon and phonon-electron scattering, *J. Appl. Phys.* **119**, 225109 (2016).
- [39] P. M. Morse and H. Feschbach, *Methods of Theoretical Physics, Parts I and II* (McGraw-Hill Book Company, New York, 1953).
- [40] As shown in the Appendix each solution also contains a short-scale low amplitude component. These components can be neglected when considering temperature variations and their role is to satisfy the vanishing thermal flux conditions at the metal-dielectric interface.
- [41] D. Marcuse, *Theory of Dielectric Optical Waveguides* (Academic Press, New York, London, 1974).
- [42] Note that Eq. (2) of Ref. [30] apparently contains a typo.
- [43] Z. Lin and L. V. Zhigilei, Thermal excitation of d-band electrons in au: Implications for laser-induced phase transformations, *Proc. SPIE* **6261**, 62610U (2006).
- [44] T. Stoll, P. Maioli, A. Crut, N. D. Fatti, C. Voisin, and F. Vallee, Advances in femto-nano-optics: Ultrafast nonlinearity of metal nanoparticles, *Eur. Phys. J. B* **87**, 260 (2014).
- [45] R. El-Ganainy, K. Makris, M. Khajavikhan, Z. Musslimani, S. Rotter, and D. Christodoulides, Non-Hermitian physics and Pt symmetry, *Nat. Phys.* **14**, 11 (2017).